# Exploring magnetic self-assembly by studying the influence of shape on interactions of centimeter size particles

G.H. Marsman

University of Twente, March 25, 2013

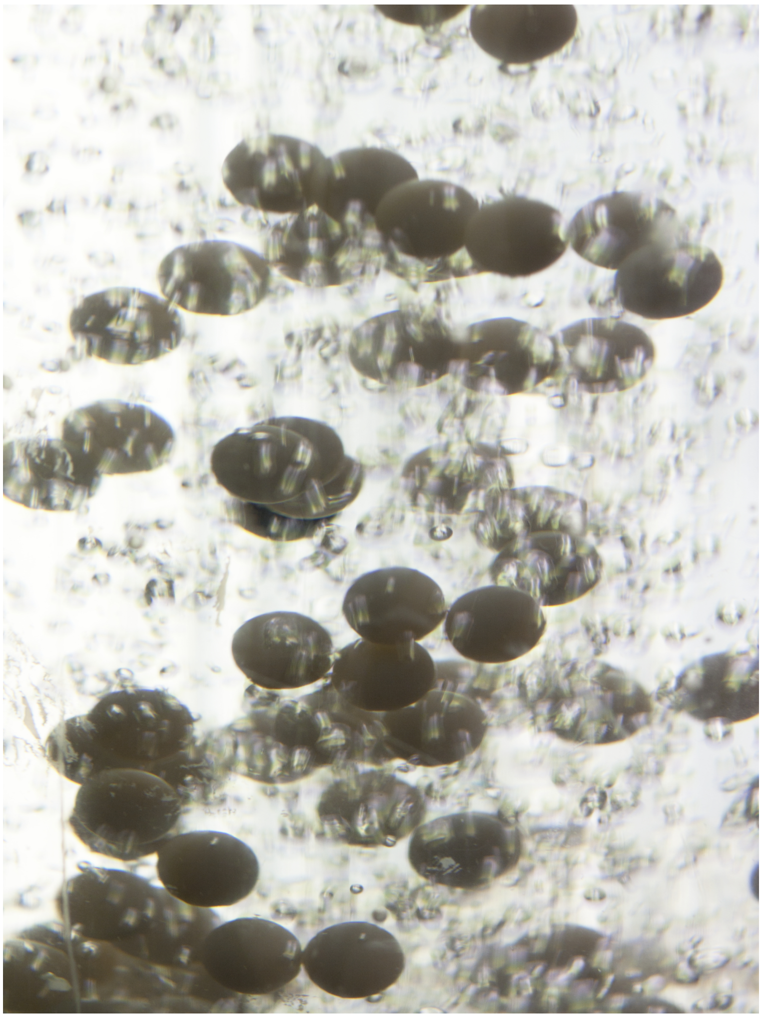

*Supervisors:*
Prof. Dr. Ir. M.C. Elwenspoek
Dr. Ir. L. Abelmann
Dr. Ing. L.A. Woldering
Dr. Ir. W. K. den Otter

**Abstract**

In this report we study how the shape of magnetic particles influences their interaction and therefore the resulting self-assembled structure. To do this a self-assembly setup is build for centimeter size magnetic particle. In the self-assembly setup air bubbles create a turbulent flow in water, which is used as distorting energy for the self-assembly process. The particles are made of small magnets enclosed in a 3D printed shell. Different shapes of particles are modeled, made and tested.

# 1 Introduction

With the current standard cleanroom technology it is possible to create a wide variety of micro and nano structures. These structures have two things in common. First they are made using photolithography, which limits the height of the structures. Building a 3D structure requires a lot of layers, which makes the production slow and expensive. Secondly these structures need to be fixed on a larger structure, normally the bulk material, for processing or assembly. This is because the structures are too small to handle using standard techniques[1].
Self-assembly has the promise to overcome these limitations. With self-assembly it will be possible to create 3D structures, which opens up a large scale of new possibilities, from smart metamaterials, like photonic crystals, to 3D electronics or 3D memory. The assembly of large amounts of small parts is possible, because in a self-assembly system the parts are not assembled one by one, but by a random process[1]. The exact position of each part at the start and during the process is not important, because the process is designed in such way that the favorable lowest energy position is the wanted assembly position.
A major step in designing a self-assembly system is the control of the particle interaction. In this report, we study the influence of shape on the interaction of centimeter size magnetic particles. The particles consist of a small neodymium magnet in a plastic shell. The use of magnetic particles for self-assembly has clear advantages; relatively large force range, well defined interaction between magnets and the plastic shell does not influence the magnetic field.
Magnets have a chain structure as preferred self-assembly structure[2]. Changing the shape of the particle will change the particle interaction and so the resulting structure, possible a 3D structure. The magnetic particles are centimeter size, the plastic shell is printed with a 3D printer, with the assistance of technician ing. G. te Riet o/g Scholten from the Robotics and Mechatronics group at the University of Twente. The use of rapid prototyping fabrication gives highly flexible and fast production of particles with arbitrary shape.

In this report we will look first into the self-assembly process and the interaction of magnetic particle. From that we design a self-assembly setup and several particle shapes. With the self-assembly setup measurements are done to verify the self-assembly process and the influence of shape on interactions of particles.

## 2 Theory

### 2.1 Self-assembly

Self-assembly is a process where from randomness a structure is created. In our report the influence of the shape of particles on the resulting structure is studied. A SA process consist of four aspects[3]; particles, binding energy, distortion energy and environment. These aspects have to be tuned specifically to make a SA process work. The magnetic energy from the magnets in the particles is the binding energy. This magnetic energy has to overcome gravity and has to be proportioned to the distorting energy. The distorting energy causes the random movement of the particles. Nature provides with thermal energy an ideal distorting energy, which is used in nano scale SA. Larger, $1cm$ sized particles are moving much slower and the gravity will dominate the large particle movement. To overcome gravity the distorting energy has to be so high, the particles will be damaged[4]. To solve these problems a turbulent flow in water is used. This lowers the influence of gravity and a distorting energy larger than the thermal energy is possible.

### 2.2 Shape dependence of the magnetic interaction

The magnetic energy is calculated using the dipole model, the magnets inside particles are considered small in comparison to distance to each other. The dipole model is used to calculate the magnetic energy[5]. Calculating the magnetic energy for spheres at different positions is used to find the lowest energy configuration, see figure 1. The series, chain, configuration is the lowest energy configuration, as expected[2]. Doing the same calculation for a particle with a 45° slope, the lowest energy position has shifted about $3mm$ to the right, as shown in figure 1. The shift depends on the angle of the slope, this is shown in figure 2. This can be used to control the particle interaction.

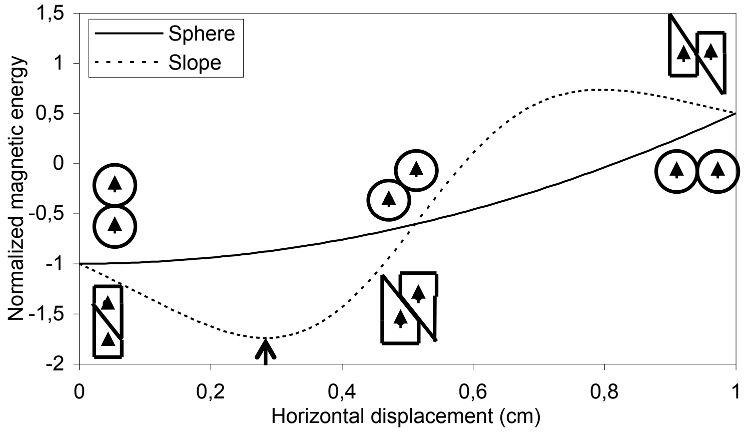


Figure 1: Magnetic energy dependence on particle shape and position. Both particles have a $1cm$ dipole distance at $0cm$ horizontal displacement. A particle with a 45° slope has a different lowest energy position, compared to a spherical particle. The arrow shows the minimum energy position.

Changing the shape of the particles can give a different lowest energy position, but the non spherical particles have more possible stable configurations. Possible other stable configurations of sloped particles and their magnetic energies are shown in table 1. Configurations 2 and 3 have the lowest magnetic energies. Which means these two configurations will occur the most. With the magnetic energies known, the chance of assembly of each configuration can be calculated at different angles, shown in table 2 and figure 3.

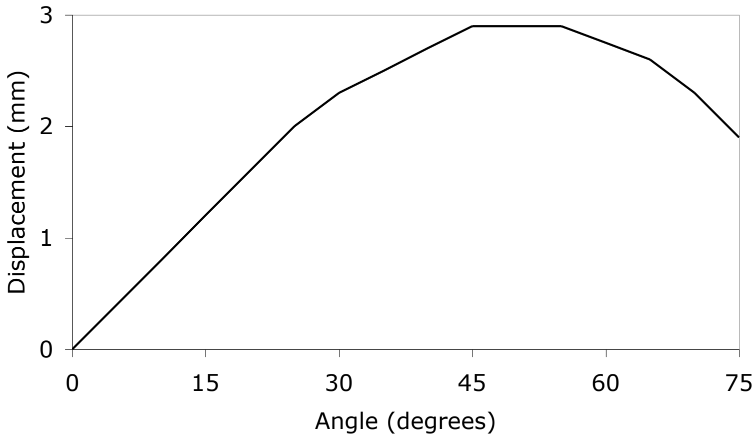


Figure 2: The horizontal displacement of configurations 2 from table 1 for different slope angles.

| Slope | 1 | 2 | 3 | 4 | 5 |
|---|---|---|---|---|---|
| | 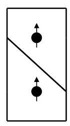 | 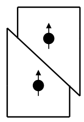 | 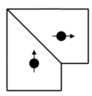 | 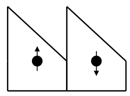 | 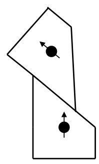 |
| | $\mu J$ | $\mu J$ | $\mu J$ | $\mu J$ | $\mu J$ |
| 15° | -8.7 | -9.1 | -9.3 | -4.3 | -4.3 |
| 30° | -8.7 | -10.8 | -11.7 | -4.3 | -5.1 |
| 45° | -8.7 | -15.1 | -18.4 | -4.3 | -6.9 |
| 60° | -8.7 | -28.2 | -43.3 | -4.3 | -10.2 |

Table 1: Magnetic energy of different configurations of particles with a slope. The magnetic energies of configurations 2 and 5 are the lowest energies of those configurations. The dipole distance of configuration 1 is $1cm$ and the dipole has the same magnetic moment as a $3mm$ magnet, $6.58\frac{mJ}{T}$.

| Slope | 2 | 3 | N2 | N3 |
|---|---|---|---|---|
| | 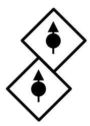 | 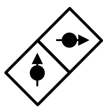 | | |
| | $\mu J$ | $\mu J$ | % | % |
| 15° | -9.1 | -9.3 | 50 | 50 |
| 30° | -10.8 | -11.7 | 48 | 52 |
| 45° | -15.1 | -18.4 | 45 | 55 |
| 60° | -28.2 | -43.3 | 37 | 63 |

Table 2: Magnetic energy and change of occurrence of configuration 2 and 3 of diamond shaped particles for different slope angles. The change of occurrence is calculated with the Boltzmann factor. For each angle the value of $kT$ is the lowest binding energy.

Another way to change preferred configuration is to use elliptical particles. With an ellipse the magnetic energies of the series and antiparallel configurations can be set individually. At one length/width ratio the magnetic energies of the series and antiparallel configurations are the same, shown in table 3. The chance of occurrence is the same for both configurations, shown in figure 4. Which means that other structure than a chain can be possible.

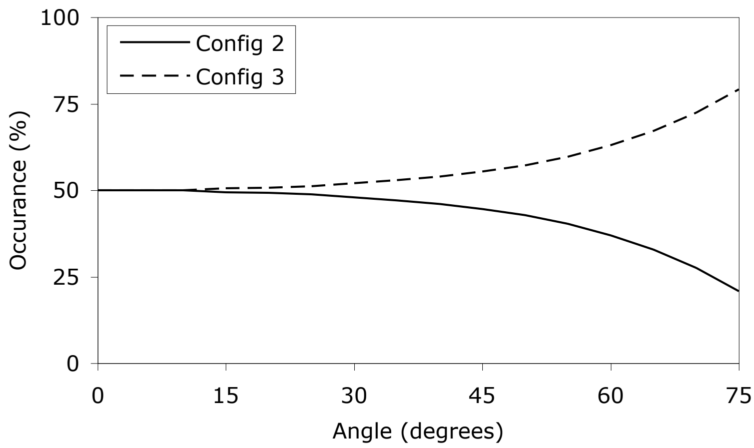


Figure 3: The chance of assembly of configurations 2 and 3 from table 1 for different slope angles.

The next step is to find structures to make with the magnetic particles. Crystal lattices have the ideal properties for SA; a regular 3D structure made of the same particles. In the appendix 7.2 calculation of unit cells are shown. The dipole calculation show a stable unit cel of a stretched diamond lattice and compressed HCP/FCC lattice.

| length $cm$ | diameter $cm$ | size ratio | 1 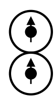 $\mu J$ | 2 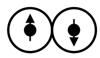 $\mu J$ |
|---|---|---|---|---|
| 1.00 | 1.00 | 1:1 | -8.7 | -4.3 |
| 1.15 | 1.00 | 1.15:1 | -5.7 | -4.3 |
| 1.26 | 1.00 | 1.26:1 | -4.3 | -4.3 |
| 1.48 | 1.00 | 1.48:1 | -2,7 | -4.3 |
| 2.05 | 1.00 | 2.05:1 | -1.0 | -4.3 |

Table 3: The magnetic energy ratios of a sphere and ellipses. The size ratio determines the energy ratio, which determine the preferable configuration.

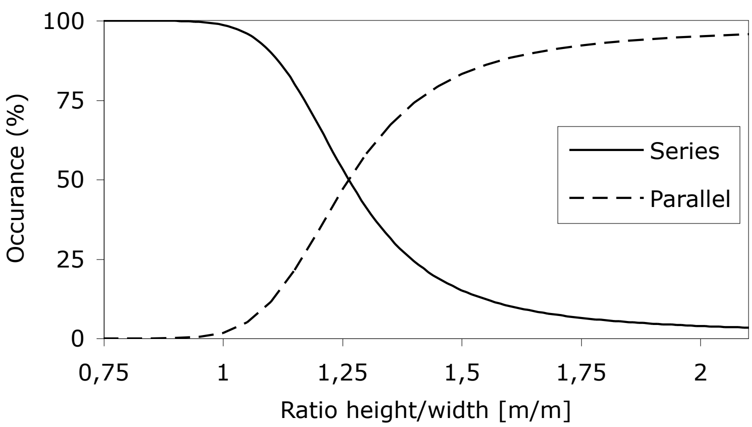


Figure 4: The occurrence of the series and antiparallel configuration depending on the size ratio of the ellipses. The occurrence is calculated with the Boltzmann factor. For each size ratio the value of $kT$ is the lowest binding energy.

## 2.3 Distorting energy

In our system the distorting energy comes from air bubbles, shown in figure 6. These air bubbles rise to the top, creating a turbulent flow. The turbulent flow is a substitute for the thermal energy. Instead of atom collisions, a turbulent flow will move the particles. The collisions of air bubbles with the particle is assumed to be negligible. The power of the turbulent flow in the system comes from the change in potential energy of the bubbles when moving upwards. Assuming the bubbles move at terminal velocity, all of the potential energy of a bubble is converted to the turbulent flow. From these assumptions follows that the power of the turbulent flow is linear dependent on the airflow.

$$P_{\text{flow}} = E_{\text{b,bubble}} k_{\text{bubble}} = \rho_{\text{solution}} g h_{\text{tube}} Q_{\text{air}} \tag{1}$$

Where $P_{\text{flow}}$ is the power of the turbulent flow, $E_{\text{b,bubble}}$ is the Buoyancy energy of a bubble, $k_{\text{bubble}}$ is the bubble rate, $\rho_{\text{solution}}$ is the density of water with bubbles, g is the gravity constant, $h_{\text{tube}}$ is the height of the inner-tube and $Q_{\text{air}}$ is the airflow. The turbulent flow created by a bubble is over time dissipated into heat, with time constant $\tau_{\text{flow}}$. The particles are pushed by the drag force from the turbulent flow. The kinetic energy of the particle depends on the drag from the turbulent flow. It is assumed that not all the energy of the turbulent flow will become kinetic energy of the particle, because of the shape of the particles.

$$E_{\text{kin}} = C_{\text{D}} P_{\text{flow}} \tau_{\text{flow}} \tag{2}$$

Where $E_{\text{kin}}$ is the average kinetic energy of a particle and $C_{\text{D}}$ is the drag coefficient of a particle. The kinetic energy of the particle due to the turbulent flow is the distorting energy. The turbulent flow is assumed to substitute the thermal energy[6], so the airflow is related to an effective temperature.

$$E_{\text{kin}} = \frac{1}{2} m v^2 = \frac{3}{2} k T_{\text{eff}} = \frac{3}{2} a \ Q_{\text{air}} \tag{3}$$

$$a = \frac{2}{3} C_{\text{D}} \rho_{\text{solution}} g h_{\text{tube}} \tau_{\text{flow}} \tag{4}$$

The $E_{\text{kin}}$ is linear depended on the airflow, with fitting parameter $a$. The $\tau_{\text{flow}}$ is an unknown constant, therefore the $kT_{\text{eff}}$ has to be measured. One way to determine $kT_{\text{eff}}$ is to measure the average height. The height of the particles depends on the turbulent flow and gravity. The number of particles to be at a certain height is exponential distributed[6].

$$\frac{c(h)}{c(0)} = exp(-h \frac{F_{\text{g,particle}} - F_{\text{b,particle}} - F_{\text{d,particle}}}{kT_{\text{eff}}}) \tag{5}$$

Where $c(0)$ is the concentration at the bottom, $c(h)$ is the concentration at height $h$, $F_{\text{g,particle}}$ is the gravity force on the particle, $F_{\text{b,particle}}$ is buoyancy force on the particle and $F_{\text{d,particle}}$ is drag force of the water flow on the particle. The water flow in the SA setup comes from the density difference between water with bubbles inside the inner-tube and water outside the inner-tube. When the drag of the water flow becomes larger than the gravity minus the buoyancy, the particles start to float to the top and the concentration distribution inverses. At the moment the gravity, buoyancy and drag are canceling each other out, the most particles will be suspended between the top and the bottom. Which is the ideal circumstance for SA.
From the height distribution of the particles the expected height can be derived.

$$H(c(h)) = \frac{kT_{\text{eff}}}{F_{\text{g,particle}} - F_{\text{b,particle}} - F_{\text{d,particle}}} \tag{6}$$

To use the expected height, $H(c(h))$, for determining $kT_{\text{eff}}$, the buoyancy force on the particle has be determined first.

$$F_{\mathrm{b,particle}} = V_{\mathrm{particle}}\rho_{\mathrm{solution}}g \tag{7}$$

Where $V_{\mathrm{particle}}$ is the volume of the particle. The buoyancy force depends on the density of water with bubbles.

$$\rho_{\mathrm{solution}} = \rho_{\mathrm{water}} - (\rho_{\mathrm{water}} - \rho_{\mathrm{air}})\frac{V_{\mathrm{air}}}{V_{\mathrm{tube}}} \tag{8}$$

Where $V_{\mathrm{air}}$ is volume of air in the inner-tube, $V_{\mathrm{tube}}$ is the volume of the inner-tube, $\rho_{\mathrm{water}}$ and $\rho_{\mathrm{air}}$ are the density of water and air respectively. $V_{\mathrm{air}}$ can be determined from the time it takes for a bubble to rise from the bottom to the top of the inner-tube and the total volume bubbles created each second, the airflow. The $\rho_{\mathrm{solution}}$ is linear dependent on the airflow.

$$V_{\mathrm{air}} = \frac{h_{\mathrm{tube}}}{v_{\mathrm{T}}}Q_{\mathrm{air}} \tag{9}$$

$$\rho_{\mathrm{solution}} = \rho_{\mathrm{water}} - b\ Q_{\mathrm{air}} \tag{10}$$

$$b = (\rho_{\mathrm{water}} - \rho_{\mathrm{air}})\frac{h_{\mathrm{tube}}}{v_{\mathrm{T}}V_{\mathrm{tube}}} \tag{11}$$

Where $v_{\mathrm{T}}$ is terminal velocity of a bubble and $b$ is a fitting parameter. The buoyancy force on a particle is determined. The drag force on the particle is the last undetermined part of the expected height equation. During experiments the water flow will be close to thermal velocity of the particles, so quadratic drag is assumed[7].

$$F_{\mathrm{d,particle}} = \frac{1}{2}C_{\mathrm{D}}\rho_{\mathrm{solution}}\pi r_{\mathrm{particle}}^2 v_{\mathrm{water}}^2 \tag{12}$$

Where $r_{\mathrm{particle}}$ is the radius of the particle and $v_{\mathrm{water}}$ is the velocity of the water. The velocity of water depends on the airflow. When the airflow increases, $\rho_{\mathrm{solution}}$ decreases and $v_{\mathrm{water}}$ increases. If the airflow is constant $v_{\mathrm{water}}$ will be constant, which means the buoyancy, gravity and drag force on the water with bubbles are in equilibrium.

$$F_{\mathrm{b,solution}} - F_{\mathrm{g,solution}} = F_{\mathrm{d,tube}} \tag{13}$$

Where $F_{\mathrm{b,solution}}$ is buoyancy force, $F_{\mathrm{g,solution}}$ is the gravity force and $F_{\mathrm{d,tube}}$ is the drag force of the water with bubbles in the inner-tube. This equation can be written out in parameters $Q_{\mathrm{air}}$ and $v_{\mathrm{water}}$.

$$(\rho_{\mathrm{water}} - \rho_{\mathrm{air}})\frac{h_{\mathrm{tube}}}{v_{\mathrm{T}}}gQ_{\mathrm{air}} = \frac{1}{2}C_{\mathrm{D,tube}}\rho_{\mathrm{solution}}\pi r_{\mathrm{tube}}^2 v_{\mathrm{water}}^2 \tag{14}$$

Where $C_{\mathrm{D,tube}}$ is the drag coefficient and $r_{\mathrm{tube}}$ is the radius of the inner-tube. The $C_{\mathrm{D,tube}}$ is unknown, because this drag coefficient comes from the inlet, outlet and wall flow resistance of the inner-pipe. The equation can be reduce to parameters $v_{\mathrm{water}}$, $Q_{\mathrm{air}}$ and fitting parameter $c$.

$$v_{\mathrm{water}}^2 = c\ Q_{\mathrm{air}} \tag{15}$$

$$c = 2\frac{(\rho_{\mathrm{water}} - \rho_{\mathrm{air}})h_{\mathrm{tube}}g}{C_{\mathrm{D,tube}}\rho_{\mathrm{solution}}\pi r_{\mathrm{tube}}^2 v_{\mathrm{T}}} \tag{16}$$

$$H(c(h)) = \frac{a\ Q_{\text{air}}}{m_{\text{particle}} g - (\rho_{\text{water}} - b\ Q_{\text{air}}) V_{\text{particle}} g - \frac{1}{2} C_{\text{D}} (\rho_{\text{water}} - b\ Q_{\text{air}}) \pi r_{\text{particle}}^2 c\ Q_{\text{air}}} \tag{17}$$

Where $m_{\text{particle}}$ is the mass of the particle. The model for the expected height of a particle is complete. This model can be fitted to the measured average height of a particle to determine the $kT_{\text{eff}}$.

## 2.4 Interaction of 2 particles in a SA system

The interaction of 2 particles in a SA system can be described with 2 states; together and separated. The distorting energy causes the 2 particles to switch states. The amount of airflow determines the chance the particles will be in one state or the other.
This interaction is comparable with a simple chemical reaction in equilibrium, but in stead of measuring the amount of atoms reacted or not reacted, the amount of times the particles being are in one state or the other is measured at a set airflow. The interaction of 2 particles can also be described with an equilibrium coefficient, $K$.

$$K = \frac{N_{\circ\leftrightarrow\circ}}{N_{\circ\circ}} = \frac{k_{\text{separation}}}{k_{\text{combination}}} \tag{18}$$

Where $N_{\circ\leftrightarrow\circ}$ and $N_{\circ\circ}$ are the number of times the 2 particles are separated or together respectively, $k_{\text{separation}}$ and $k_{\text{combination}}$ are the separation rate and combination rate. The $k_{\text{separation}}$ can be described with the Arrhenius equation. The separation of particles is caused by random flow, which is comparable with a bi-atomic gas[6]. There is no Gibbs free energy of activation, because there is no transition state. The average kinetic energy of 2 combined particles is twice the average kinetic energy of 1 particle. Half of the kinetic energy of 2 combined particles is the center-of-mass motion and the other half is vibrational and rotational motion. The center-of-mass motion is the motion of the two particles in the same direction. Vibrational and rotational motion is the different in motion of one particle to the other, this motion causes the particles to separate.

$$k_{\text{separation}} = A\ exp(-\frac{E_{\text{M}}}{kT_{\text{eff}}}) \tag{19}$$

Where A is the pre-exponential factor and $E_{\text{M}}$ is magnetic energy. The $k_{\text{combination}}$ is different from a simple chemical reaction. There is no activation energy for combining 2 particles. The $k_{\text{combination}}$ is the attempt frequency, so $k_{\text{combination}}$ depends only on the diffusion of the particles and the mean free path. The diffusion is determined by the Einstein relation[4]. The mean free path is the average distance between collisions.

$$k_{\text{combination}} = \frac{6D}{l^2} = \frac{kT_{\text{eff}}}{\pi\eta r_{\text{particle}} l^2} \tag{20}$$

Where $D$ is the diffusion, $l$ is the mean free path, $\eta$ is the dynamic viscosity of the medium and $r_{\text{particle}}$ is the radius of the particle. The mean free path is distance a particle travels so that expected number of collisions is one.

$$l = \frac{V_{\text{tube}}}{\pi r_{\text{collision}}^2} \tag{21}$$

Where $r_{\text{collision}}$ is the collision radius. Normally $r_{\text{collision}}$ is the radius of the particle, but because of the magnetic field $r_{\text{collision}}$ is larger than $r_{\text{particle}}$. The distance where the two particles become trapped in each others magnetic field and attracted to each other is $r_{\text{collision}}$.

# 3 Design

## 3.1 Particles

The particles are made by glueing a neodymium magnet between two 3D printed halves, shown in figure 5. The N35 neodymium magnets used for the experiments have a diameter of $3mm$ and $4mm$, a height of $1mm$ and a magnetic flux density of $1.17T$[8]. These magnets are chosen, because of their low weight and being strong enough to keep particles together in water.
The two plastic halves are printed with an Objet Eden250$^{TM}$ 3D printer, with a $\leq 85\mu m$ resolution[9]. The material used is VeroWhite FullCure830 plastic. This plastic is non magnetic. The shapes printed for the experiments are described in appendix 7.1 table 6.

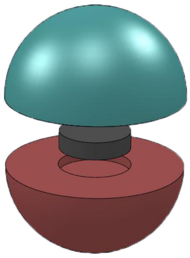

Figure 5: Exploded view of a spherical particle. A neodymium magnet is enclosed within 3D printed shapes.

## 3.2 Self assembly setup

The SA setup consist of two perspex tubes. One fitted inside the other, shown in figure 6. The SA takes place inside the inner-tube. This inner-tube is put on legs to ensure the inflow of water and air bubbles. The air bubbles come from an aquarium air stone disc, creating bubbles with a size about $3mm$[10]. The air is compressed air regulated by a Bronkhorst EL-FLOW F-201C-FA-22-V mass flow controller. The water used is tap water at ambient temperature.

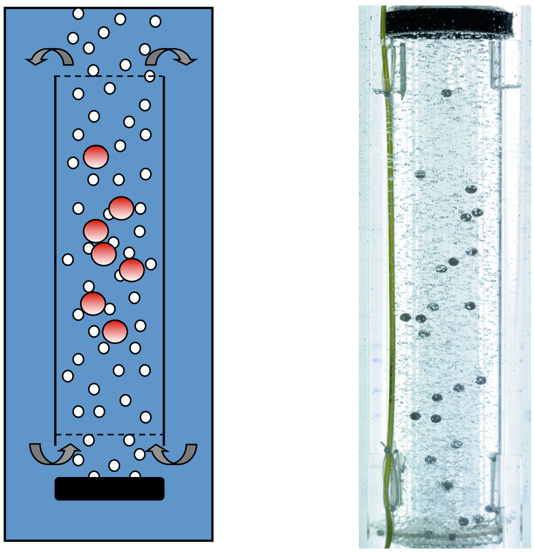

Figure 6: On the left side a schematic of the SA setup and on the right side a photo of the setup. The inner-tube has an outer-diameter of $100mm$, a wall thickness of $5mm$ and is $585mm$ long. At the top and bottom of the inner-tube grating is placed to keep the particles inside. The air stone disc has a diameter of $110mm$. The outer-tube has an outer-diameter of $200mm$, a wall thickness of $5mm$ and is $850mm$ long. The particles in the photo are spheres without a magnet.

# 4 Experiments

## 4.1 Shape interaction

The interaction of particles is observed by taking photos of the particles at an airflow where the particles continuously separate and combine. This optimal airflow depends on the shape of the particle. First the tetrapod particle, specified in table 6, are observed. They form only chain structures, a photo is shown in figure 7. No 2D or 3D structures are observed. Each tetrapod particle combined with only two other particles.
Second the particles with a sloped surface of 15°, 30°, 45° and 60° are observed, one photo is shown in figure 8. These particles form two configurations; configuration 2 and 3 from table 1. The particle with a 60° slope started in a few occasions to spin around the vertical axis, due to the asymmetrical shape in the upward water flow.
Next the diamond shaped particles, specified in table 6 are observed, shown in figure 9. The diamond particles form only chain structures using also configurations 2 and 3.

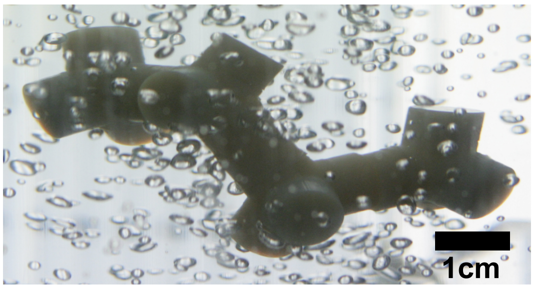


Figure 7: A photo of four tetrapods forming a chain structure.

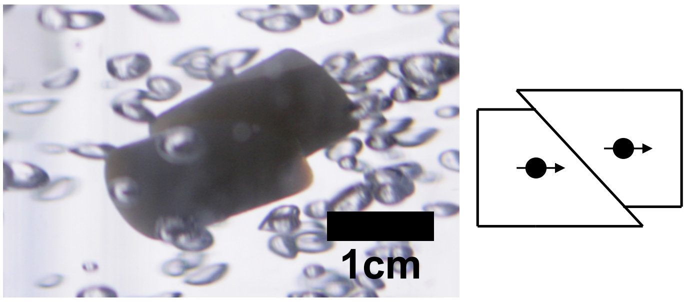


Figure 8: A photo and a schematic representation of two particles with a 45° slope forming configuration 2 of table 1.

The last particles observed are the spherical and ellipsoidal particles, specified in table 3 and table 6. These particles are forming chain structures. The two largest ellipsoidal particles are forming only chain structures in antiparallel configuration, a photo is shown in in figure 10. The other smaller particles are forming only chain in series configuration, a photo is shown in in figure 11. The expected transition where both series and antiparallel configurations should occur, shown in figure 4 , is not observed.

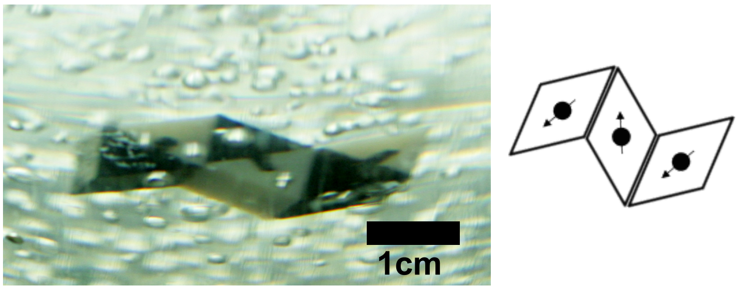


Figure 9: A photo and a schematic representation of three diamond particles with a 60° slope forming a chain structure. Each connection is the lowest energy configuration, configuration 3 of table 1. The magnetic north pole is shown by the black half of the particle.


Figure 10: A photo and a schematic representation of five ellipses forming a chain sideways. The ellipses are $1cm$ in diameter and $2.05cm$ long. This configurations is the lowest energy configuration, calculated in table 3.

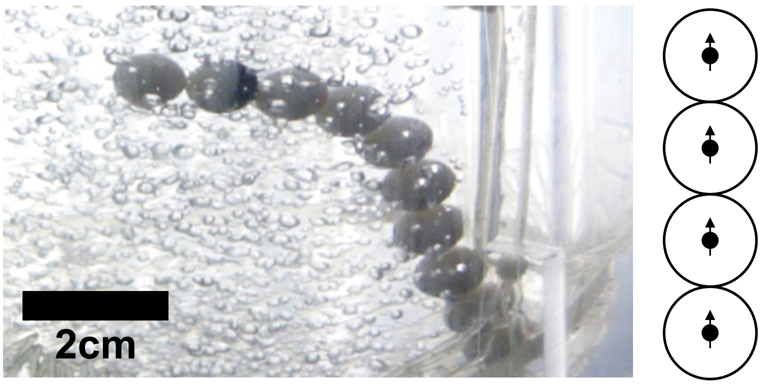


Figure 11: A photo and a schematic representation of ten sphere forming a chain structure. The black half of a sphere shows the magnetic north pole of the particle.

## 4.2 Determining the distorting energy

The distorting energy cannot be measured directly. The distorting energy can be derived from fitting the average height and N=2 interaction models to measurements. First the height measurement is described and secondly the N=2 interaction measurement.
Before doing the height measurement the density of the water with bubbles at different airflows have to be measured. The density measurements are done by lifting the inner-tube partly above water at a set airflow. If the inner-tube is lifted until the water stops flowing, the water with bubbles level is higher than the water level. Archimedes' principle dictates that at this point the weight of the water with

bubbles in the inner-tube is the same as the weight of water of the inner-tube volume underwater. The height of the inner-tube above water is measured, from this the volume of the inner-tube underwater is determined and so the density of water with bubbles. This is done for different airflow rates, resulting in figure 12.

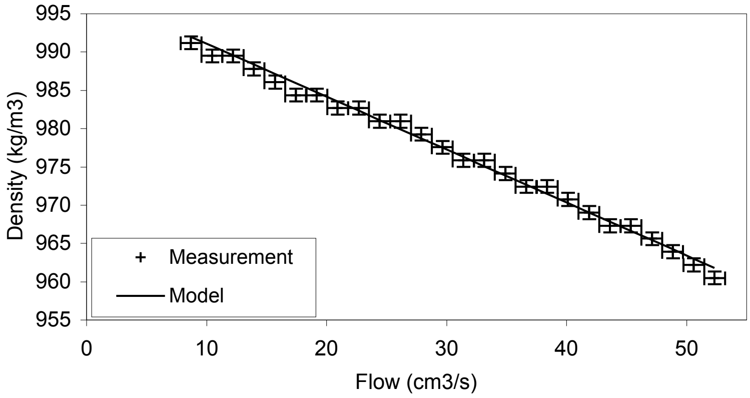


Figure 12: Density measurement of water with bubbles at different flows. The analytic model, equation 10, fitted to the measurement within the measurement error. The fitted $\rho_{\text{water}} = 997.4 \pm 0.4\frac{kg}{m^3}$, fitting parameter b $= 6.8{\cdot}10^5 \pm 0.1{\cdot}10^5\frac{kg\ s}{m^6}$ and a $R^2$ of 0.994. The airflow is compensated for the temperature and pressure. The measurement error are $\pm\ 0.87\frac{cm^3}{s}$ for the airflow and $\pm\ 0.5mm$ or $\pm\ 0.85\frac{kg}{m^3}$ for measuring the height.

The height measurement are done by taking multiple photos of one spherical particle. At each airflow rate 100 photos are taken with a 5 seconds intervals. From each photo the height is measured. The number of times the particle is in a $2.5cm$ height bin is shown in figure 13. This height measurement is done with three different spherical particles; without a magnet, $3mm$ magnet and $4mm$ magnet. These particles where chosen, because they have the same volume and shape, but they differ in weight.

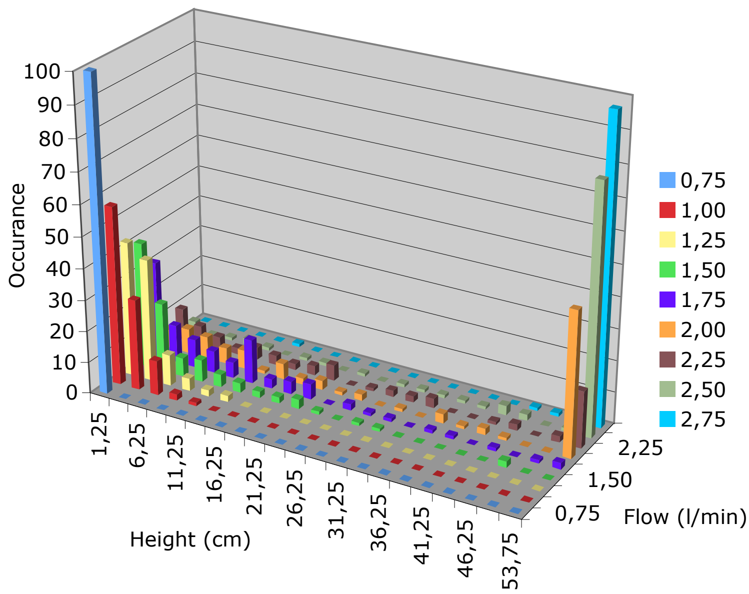


Figure 13: Height distribution of a sphere with a $3mm$ magnet at different flows. The photos are taken with a shutter speed of $1ms$ or faster, to ensure freezing the movement of the particle for the height measurement. The legend states the set airflow in $\frac{l}{min}$.

The measurements show a transition from the particle being mostly at the bottom to being mostly at the top. The particle start to float to the top, because the drag force from the water flow becomes larger than the effective gravity force. For calculating the average height only the airflow rates are used, where the particles are not at the top, shown in figure 14. The expected height model, equation 17, is fitted to the average height measurement. The fitting parameters a and c for respectively $kT_{\text{eff}}$ and $v^2_{\text{water}}$ parameters in the model are in table 4.

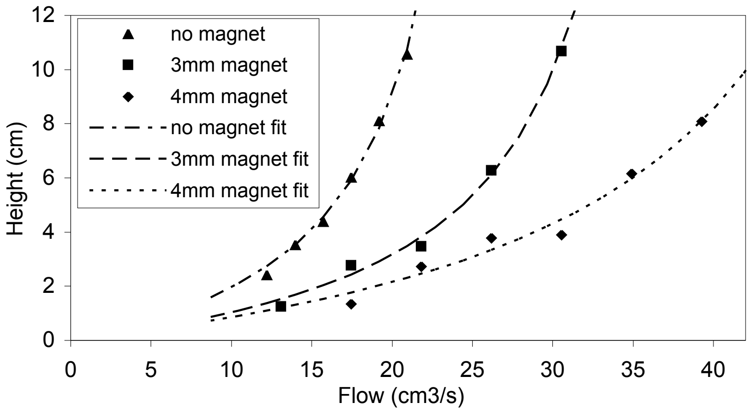


Figure 14: Average height measurement of spheres without, with a $3mm$ and a $4mm$ magnet, calculated from height measurements, one is shown in figure 13 The expected height model, equation 17, is fitted to the measurement, results are in table 4. The measurement errors are $\pm$ $0.087\frac{cm^3}{s}$ for the airflow and $\pm$ $0.125cm$ for average height.

| Particle | a $\frac{J\ s}{m^3}$ | c $\frac{1}{m\ s}$ | $\frac{Chi^2}{Dof}$ |
|---|---|---|---|
| none | 1.06 $\pm$ 0.05 | 2123 $\pm$ 38 | $6{\cdot}10^{-6}$ |
| 3mm | 0.97 $\pm$ 0.08 | 2252 $\pm$ 53 | $1{\cdot}10^{-5}$ |
| 4mm | 1.15 $\pm$ 0.15 | 1910 $\pm$ 137 | $2{\cdot}10^{-5}$ |

Table 4: The fitting parameters $a$ and $c$ from the expected height model for spherical particles, equation 17 and figure 14. The $v_{\text{T}}$ of the air bubbles used in the calculation is $0.23\frac{m}{s}$ [10]. The value for $C_{\text{D}}$ is 0.42, this is derived from a terminal velocity measurement of a sphere without a magnet. For b the measured value is used from the density measurement, see figure 12.

The interaction of two particles is measured by making photos. At each airflow rate 100 photos are taken with 5 seconds intervals. From each photo the state, combined or separated, of the particle is determined. The results are shown in figure 15. The measurements where repeated to investigate the repeatability of the results.
The particles used are the spherical particle with a $3mm$ magnet and the smallest ellipsoidal particle with a $3mm$ magnet and a length of $1.15cm$. These particle where used, because the state change happens within the useable airflow and they are similar except for the magnetic force. The N=2 model, equation 18, is fitted to the $K$ values calculated from each point, shown in figure 16. The fitted pre-exponential factor and a parameter are in table 5. The $r_{\text{collision}}$ is determined by when two particle are trapped in each other magnetic field. During terminal velocity measurement of the particles, the magnetic particles rotated to align with earth's magnetic field. For two particles to attract each other, the magnetic field of the magnetic particles has to be at least as strong as the earth's magnetic field. This is because if the magnetic field of the magnet is as strong as earth's magnetic field, the particles start to rotate to align their magnetic fields. By aligning the magnetic field the particles become more attracted to each other. The distance that the magnetic field of the magnet is as strong as earth's magnetic field, is chosen as $r_{\text{collision}}$. The $r_{\text{collision}}$ = $3cm$ for a particle with a $3mm$ magnet.

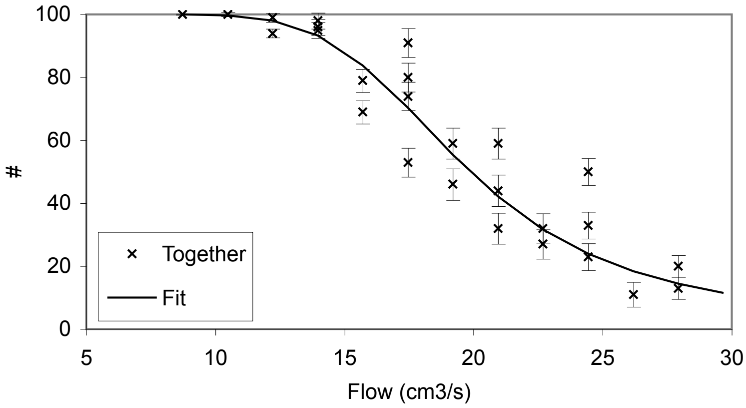


Figure 15: The measured occurrence of the together state of 2 spheres with a 3mm magnet for different flows. The fit line is derived from the N=2 model fit, equation 18, to the measured $K$ in table 5 and figure 16. The measurement error is $\pm\ 0.087\frac{cm^3}{s}$ for the airflow and the standard deviation of the occurrence.

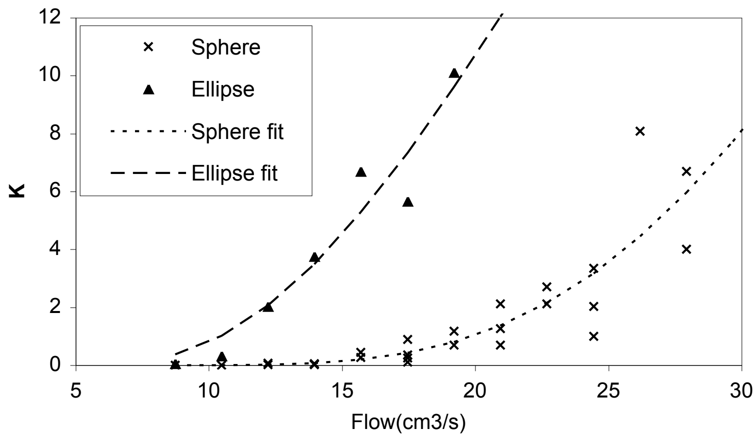


Figure 16: Equilibrium constant, $K$, measurements and N=2 model fit, equation 18, of 2 spheres and 2 ellipses with a 3mm magnet. The fit parameters are in table 5.

| Particle | A<br>Hz | a<br>$\frac{J\ s}{m^3}$ | $\frac{Chi^2}{Dof}$ |
|---|---|---|---|
| Ellipse | 18 $\pm$ 8 | 0.085 $\pm$ 0.013 | 1.1 |
| Sphere | 64 $\pm$ 52 | 0.059 $\pm$ 0.010 | 1.2 |

Table 5: The fitted pre-exponential factor and $a$ parameter from the N=2 model, equation 18. The measurements are shown in figure 16.

# 5 Discussion

## 5.1 Shape dependent interaction

The configurations formed with 2 particles with a sloped surface are in accordance with the magnetic energy calculation. The magnetic dipole model is suitable for predicting the preferred configuration of two particles. A disadvantage of using the dipole model for finding the preferred configuration is that for more particles the number of possible configurations increases extremely. For two sloped particle already five stable configurations exist. For finding the preferred configuration of large number of particles a different approach is needed, like Monte Carlo simulations[11].
The configurations formed with more than 2 particles are only chain structures. Other configuration are possible, like a diamond lattice with tetrapod particles, but none where observed. One explanation is if 2 particles are assembled, the relatively distant magnetic field of the 2 particle can be describe by one magnetic dipole. When a third particle approaches it will move to one of the magnetic poles of the 2 particle structure.
A way to overcome this problem is to significant raise the number of particles per volume, so short range interactions becomes dominant. The particles assemble in local magnetic energy minimum positions, because the overall energy minimum depends mainly on the limited space for the particles. Another possibility is to use a template with a strong magnetic field. The particles are attracted to the template and will form a structure at the template. The external magnetic field dominates the particle interaction. When the external field is switched off the structure remains.

The calculated transition region where ellipsoidal particles assemble in both series and antiparallel configurations is not observed. This transition region is between ellipsoidal particles with a length of $1.26cm$ and $1.48cm$. The transition region is smaller and is on a different length/width ratio than calculated. A more accurate way to calculate the transition region is to use a 3D FEM model, the dipole model does not incorporate the shape of the magnet in the energy calculations.

## 5.2 Density measurement

The density model, equation 14, is a close fit to the measurements, shown in figure 12. The model fits to the measurement with a $R^2$ of 0.994. The main causes of measurement errors are the flow controller and reading off the height of a continuously moving water surface, due to popping air bubbles.
The density model assumes a fixed terminal velocity of the air bubbles, but the water flow increase the terminal velocity. During the measurement there was no water flow, so the change in terminal velocity of the air bubbles could not be examined. If terminal velocity increases, the density of water with bubbles increases, so the density is higher than measured. The measured decrease in density for airflows from 10 to $40cm^3/s$ is about 2%. The real decrease of density of water with bubbles will be lower, but this could not be measured. For the discussion of the height measurements the change in terminal velocity of air bubbles is assumed to be negligible, because the error margins of the fitting parameters are assumed to be bigger than the error due change in terminal velocity.

## 5.3 Height measurement

The measured height distributions of the particles corresponds to the height distribution model, equation 5. The average height also corresponds with the expected height model, equation 17. The fitted average height model, parameters are in table 4, gives three values for $a$ of which the error margins overlap and three values of $c$ which are also close.
At an airflow of $20cm^3/s$ the $v_{\text{water}}$ is around $0.21\frac{m}{s}$. The terminal velocity of a particle without a magnet is measured at $0.23\frac{m}{s}$. The average height measurement, shown in figure 14, shows the highest airflow for the particle without a magnet is $21cm^3/s$, at higher airflow it floats to the top. For the particle to float to the top, the $v_{\text{water}}$ has to be the terminal velocity of the particle or higher, so the fitted expected height model, equation 17, gives an accurate value for $v_{\text{water}}$.

### 5.4 Interaction of 2 particles

A clear state change is observed which corresponds to the K model, equation 18. This means that SA works in this setup. The fitted parameters of the K model have a large error margins, due to the large spread in $K$ values. This spread does not come from measurement errors. The spread of repeated measurement is bigger than the measurement error margins. An explanation is that the distorting energy is nonuniform in the SA setup. The turbulent flow is not uniform, because for instance the water flow in the inner-tube has a flow profile, the water flow in the middle is higher than at the sidewall. Another cause is inlet of water with air bubbles. The air bubbles rise from the air stone disc and water flows from the side into the inner-tube. These aspected need to be explored further for an exact explanation.
The fitted $a$ parameter is lower than the fitted $a$ parameter of the average height measurement. At an airflow of $20cm^3/s$ the $kT_{\text{eff}}$ is around $20\mu J$ for the average height measurement and $1.7\mu J$ and $1.2\mu J$ for the ellipse and sphere respectively for the N=2 measurement. The difference can be explained by difference in vertical distorting energy and horizontal distorting energy. The average height measurement only measures the distorting energy in the vertical direction. The N=2 measurement measures the distorting energy in vertical and horizontal directions. From difference in the fitted $a$ parameter, it is expected that the distorting energy in the vertical direction is larger than the horizontal plane. This has to be explored further for an exact explanation.

The calculated magnetic energies of 2 combined particles are $5.7\mu J$ and $8.7\mu J$ for ellipses and spheres. The $kT_{\text{eff}}$ values of both measurements are relatively close. Another explanation for distorting energy is the collisions with air bubbles. Assuming an air bubble travels at terminal velocity, has a hard shell and hits a particle full on, so all the kinetic energy goes from the air bubble to the particle. For a spherical air bubble with a diameter of $3mm$ this kinetic energy is about $0.37\mu J$. The real average collision energy is much lower, because the shape of the air bubble will change on impact. Therefore the turbulent flow model give more accurate result in comparison with the collision model.
The turbulent flow is an alternative for the thermal energy. A bubble flow causing a $kT_{\text{eff}}$ of $10\mu J$ compares to a SA system based on thermal energy with an effective temperature of $7.2 \cdot 10^{17} K$.

## 6 Conclusion and Outlook

We have created functional SA setup with centimeter size magnetic particles. The SA works within a limited range of weight, drag coefficient and strength of magnetic field of the particles. The by air bubbles created turbulent flow is an alternative for the thermal energy, so the limits of relatively large scale SA system are overcome. Analytic models for distorting energy, particle height distribution and 2 particle interaction accurate describe parts of the SA setup. These models fit close to the measurements and the fit parameters have realistic values.
Calculations and experiments with sloped particles and ellipsoidal particles show how the shape of particles influences the resulting structures. Magnetic dipole calculations show magnetically stable crystal lattices, but these do not form during experiments. The only structures formed with the SA setup are chain structures, no interconnected 2D or 3D structures are formed. Two solutions for creating 2D and 3D structures with magnetic particles are significant increasing the number of particle per volume and use of an external field with a template.

This report is a first step into magnetic self-assembly. There are aspect which requires more research, the difference of distorting energy in the vertical direction and the horizontal plane, the uniformness of the turbulent flow and the velocity of the water flow. With better understanding, self-assembly can become a useful way for making structures, which are hard or impossible to make with other technologies.

## References


[1] Zheng W, Jacobs H O 2005 Fabrication of multicomponent microsystems by directed three-dimensional self-assembly *Adv. Funct. Mater.* **5** 732-738

[2] Stambaugh J, Lathrop D P, Ott E, Losert W 2003 Pattern formation in a monolayer of magnetic spheres *Phys. Rev. E* **68** 026207

[3] Pelesko J A, 2007 Self-assembly: The science of things that put themselves together *Chapman & Hall/CRC*

[4] Elwenspoek M, Abelmann L, Berenschot E, van Honschoten J, Jansen H, Tas N 2010 Self-assembly of (sub-)micron particles into supermaterials *J. of Micromechanics and Microengineering* **20** 1-28

[5] Alink L, Marsman G H, Woldering L, Abelmann L 2011 Simulating three dimensional self-assembly of shape modified particles using magnetic dipolar forces *Micromechanics and Microsystems Technology Europe Workshop* 22

[6] Feynman RP, Leighton R B, Sands M 1963 The Feynman Lectures on Physics vol. 1 *Addison-Wessley* chapters 39 to 43

[7] Feynman RP, Leighton R B, Sands M 1963 The Feynman Lectures on Physics vol. 2 *Addison-Wessley* chapter 41

[8] K&J Magnetics, Inc. magnets specification sheet http://www.kjmagnetics.com/specs.asp

[9] Objet Eden250™ specification sheet http://objet.com/sites/default/files/E250_ A4_ il.pdf

[10] Tomiyama A, Celata G B, Hosokawa S, Yoshida S 2002 Terminal velocity of single bubbles in surface tension force dominant regime *Int. J. of Multiphase Flow* **28** 1497-1519

[11] Graaf J de 2012 Anisotropic nanocolloids: self-assembly, interfacial adsorption, and electrostatic screening *Utrecht University*

# 7 Appendix

## 7.1 Fabricated particles

| Shape | Size | | Assembly | | Description |
|---|---|---|---|---|---|
| | diameter $cm$ | length $cm$ | series | anti-parallel | |
| 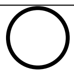 | 1 | 1 | x | | Spherical particle used in the height and interaction measurements. |
| 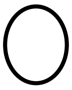 | 1 | 1.15 | x | | Ellipsoidal particle a prolate spheroid. This particle is used in the interaction measurement. |
| 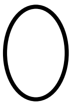 | 1 | 1.26 | x | | Ellipsoidal particle is a prolate spheroid. |
| 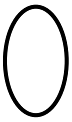 | 1 | 1.48 | | x | Ellipsoidal particle is a prolate spheroid. |
| 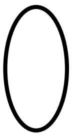 | 1 | 2.05 | | x | Ellipsoidal particle is a prolate spheroid. |
| 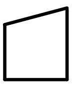 | 1 | 1.13 | x* | x* | Cylindrical particle with the top on an 15° angle. |
| 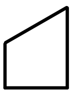 | 1 | 1.29 | x* | x* | Cylindrical particle with the top on an 30° angle. |
| 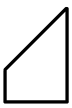 | 1 | 1.5 | x* | x* | Cylindrical particle with the top on an 45° angle. |
| 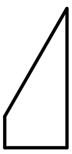 | 1 | 2.23 | x* | x* | Cylindrical particle with the top on an 60° angle. |
| 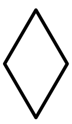 | 1x1 | 1.73 | x* | x* | Diamond particle with a square base and 60° angle sides |
| 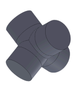 | 1** | 1.11** | x | | Tetrapod structure. It has a magnet inside in each leg. Two with the north pole pointing outwards and two with the south pole pointing outwards. |

Table 6: An overview and description of the particles used in the measurements. * The assembly of these particle are configuration 2 and 3 from table 1 instead of series and antiparallel assemblies respectively. ** The diameter of each leg is $1cm$ and the length of each leg is $1.11cm$.

## 7.2 Magnetic unit cell calculations

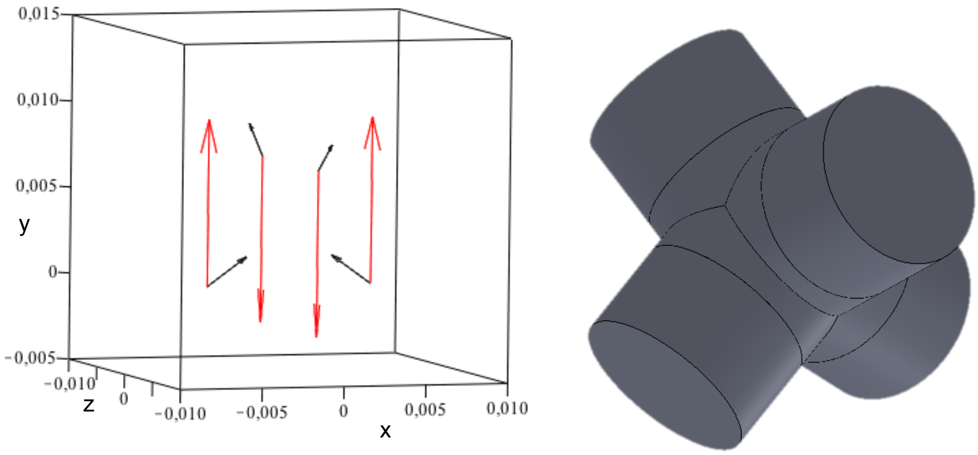


Figure 17: Four magnetic dipole forming a tetrapod. On the left side is the magnetic calculation, where the black arrows are the magnetization direction and the red arrows are the total magnetic force on each dipole. Experiment are done with particles which could form a tetrapod together. A tetrapod was never observed, probably because the magnetic force do not point to one point. For the measurements a complete tetrapod is made, shown on the right side and in figure 7.

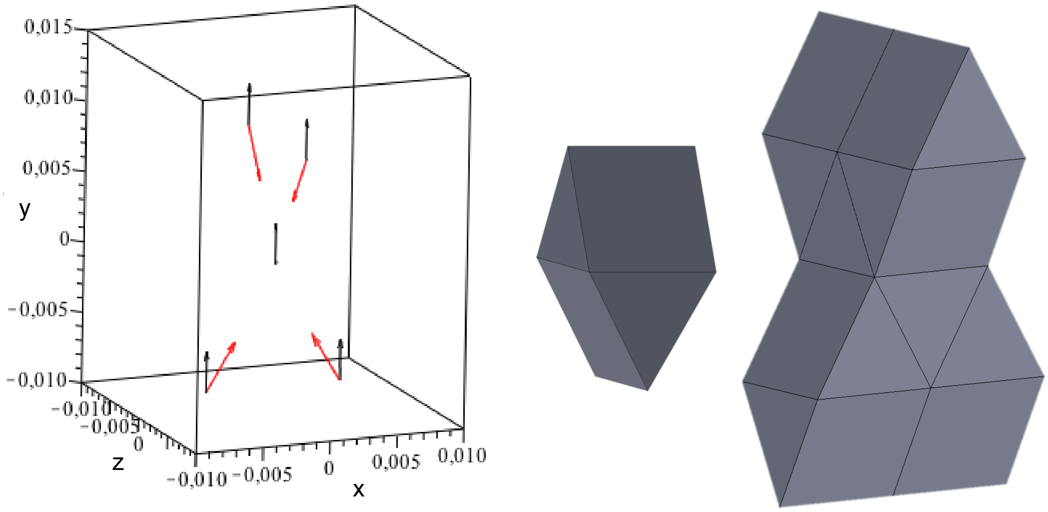


Figure 18: A stable configuration consisting of 5 magnetic dipoles. The black arrows are the magnetization direction and the red arrows are total magnetic force on each dipole. A particle which will fit in this configuration is shown in the middle. On the right side an assembly of 5 particles is shown. Assembled in a 3D structure, these particle form a diamond lattice stretched in the y direction.

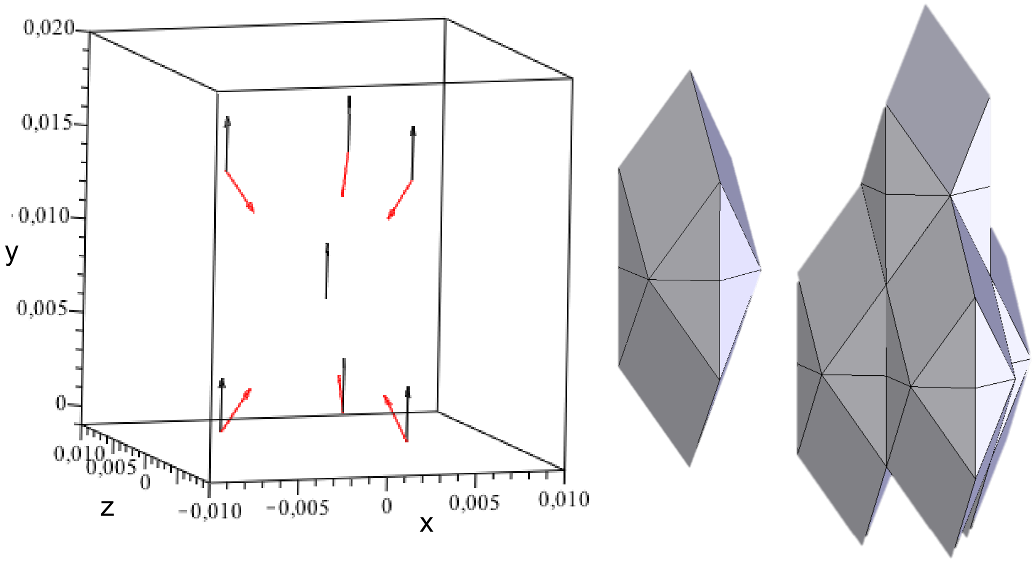


Figure 19: A stable configuration of 7 magnetic dipoles. This configuration is close a HCP, in the y direction the unit cell is shorter. In the middle a particle is shown which will fit in this configuration. On the right side an assembly of the bottom three and centre particles is shown. If the top half of the particle is rotated 60°, the particles form a FCC lattice compressed in the y direction.

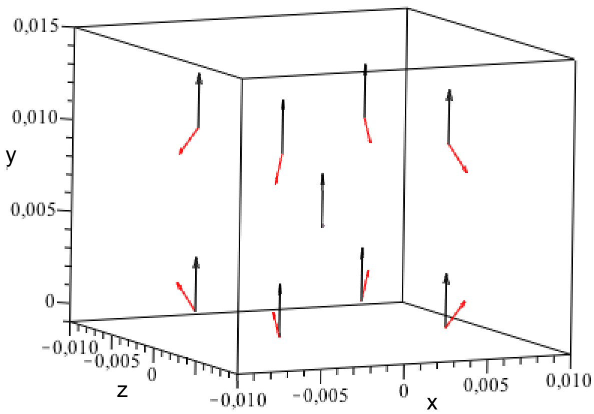


Figure 20: An unstable BCC unit cell. With our magnetic dipole calculation we could not find a stable BCC configuration.